ISSN 0915-633X

NATIONAL INSTITUTE FOR FUSION SCIENCE

Initial Value Problem of the Toroidal Ion Temperature Gradient Mode

T. Kuroda, H. Sugama, R. Kanno, M. Okamoto and W. Horton

(Received - May 14, 1998)

NIFS-551 June 1998

RESEARCH REPORT
NIFS Series

NAGOYA, JAPAN

Initial Value Problem of the Toroidal Ion Temperature Gradient Mode

T. KURODA , H SUGAMA[1], R. KANNO[1] , M. OKAMOTO[1] , and W HORTON[2]

Graduate University for Advanced Studies, Toki 509-5292
[1] *National Institute for Fusion Science, Toki 509-5292*
[2] *Institute for Fusion Studies, The University of Texas at Austin, Austin, Texas 78712, USA*

The initial value problem of the toroidal ion temperature gradient mode is studied based on the Laplace transform of the ion gyrokinetic equation and the electron Boltzmann relation with the charge neutrality condition. Due to the toroidal magnetic drift, the Laplace-transformed density and potential perturbations have a branch cut as well as poles on the complex-frequency plane. The inverse Laplace transform shows that the temporal evolution of the density and potential perturbations consists of the normal modes and the continuum mode, which correspond to contributions from the poles and the branch cut, respectively. The normal modes have exponential time dependence with the eigenfrequencies determined by the dispersion relation while the continuum mode shows power-law decay oscillation. For the stable case, the long-time asymptotic behavior of the potential and density perturbations is dominated by the continuum mode which decays slower than the normal modes.

KEYWORDS: ion temperature gradient mode, toroidal resonance, phase mixing, analytic continuation, branch cut, normal mode, continuum mode

§1. Introduction

Many works have been done on the ion temperature gradient mode (ITG mode)[1-8] because it is considered as the most likely instability to cause the anomalous ion thermal transport observed in high ion temperature plasmas. It is well-known that there are two branches of the ITG mode: the slab ITG mode and the toroidal ITG mode.[5] Because of its larger growth rate, in the present study as in most recent works, we are concerned with the toroidal ITG mode which is driven by the ion temperature gradient combined with the toroidal magnetic ∇B-curvature drift.

The kinetic dispersion relation for the toroidal ITG mode including effects of the finite gyroradius and the toroidal resonance are derived by using the gyrokinetic equation[9] for ions and the Boltzmann distribution for electrons with the charge neutrality condition Due to the quadratic form of the parallel and perpendicular velocities in the ∇B-curvature drift, the toroidal resonance has qualitatively different characteristics from the parallel drift resonance in the slab case. Thus, when we define the dispersion function on the complex-frequency ω-plane for the toroidal ITG mode, its analytic continuation requires a branch cut on the $\mathrm{Im}(\omega) < 0$ plane.[10] We need to take account of this property caused by the toroidal resonance in order to obtain the complex eigenfrequencies especially with negative imaginary parts (or negative growth rates) from the dispersion relation.[8] These eigenfrequencies ω determine the temporal behavior of the normal modes as $\propto \exp(-i\omega t)$. However, as shown by Kim *et al.*,[8] the ballistic response in the presence of the toroidal resonance shows a slow power-law decay rather than the exponential decay of stable normal modes. Therefore, description of the toroidal ITG mode only by the normal modes seems to be incomplete especially for stable systems. The power-law decay oscillation may be called continuum modes which are required for the complete representation of the initial value problem.

In this work, we direct our attention to rigorous description of temporal evolution of the toroidal ITG mode including both exponential and power-law dependence. For that purpose, the initial value problem of the toroidal ITG mode is explicitly formulated based on the Laplace transform rather than the Fourier transform. We treat appropriately a Landau contour and a branch cut for analytic continuation on the complex ω-plane by following Kim *et al.*[8] Then, we show that the density and potential perturbations of the toroidal ITG mode contain two different types of temporal behavior: the normal modes and the continuum modes which correspond to contributions from the poles and the branch cut of the Laplace-transformed potential function on the complex ω-plane, respectively. The continuum mode is shown to decay by power law like the ballistic response and dominate the asymptotic behavior of the toroidal ITG mode for the stable case.

This work is organized as follows. In Sec. 2, the ion gyrokinetic equation and its Laplace transform are presented. The ballistic response is derived from the propagator in the gyrokinetic equation, and the density perturbation decay due to the phase mixing by the parallel and toroidal drift is shown. In Sec 3, the toroidal ITG mode is formulated as an initial value problem. Analytic continuation on the complex-frequency plane for the case with the toroidal magnetic drift is reviewed. Temporal evolution of the density and potential perturbations of the toroidal ITG mode is shown to consist of the normal modes and the continuum mode. In Sec. 4, the disper-

sion relation and the initial value problem of the ITG mode are numerically solved to show the behavior of the normal and continuum modes in some examples. Finally, conclusions are given in Sec. 5.

§2. Ion Gyrokinetic Equation

2.1 Laplace transform of the gyrokinetic equation

The ion distribution function in the $(\boldsymbol{x}, \boldsymbol{v})$ phase space is divided into the equilibrium and perturbation parts as $f_i = n_0 F_M + \delta f_i$ where n_0 is the equilibrium density, $F_M \equiv \pi^{-3/2} v_{Ti}^{-3} \exp(-v^2/v_{Ti}^2)$ is the Maxwellian distribution function, and $v_{Ti} \equiv (2T_i/m_i)^{1/2}$ is the thermal velocity for the ions with the mass m_i, the temperature T_i, and the electric charge e. In the magnetic field $\boldsymbol{B}$, the perturbation part δf_i with the perpendicular wavenumber vector $\boldsymbol{k}_\perp$ is written as

$$\delta f_i = -\frac{e\phi}{T_i} n_0 F_M + h e^{-i\boldsymbol{k}_\perp \cdot \boldsymbol{\rho}} \tag{2.1}$$

where ϕ represents the electrostatic potential, $\boldsymbol{\rho} \equiv \boldsymbol{b} \times \boldsymbol{v}/\Omega_i$ $(\boldsymbol{b} = \boldsymbol{B}/B)$ denotes the ion gyroradius vector, and $\Omega_i \equiv eB/(m_i c)$ is the ion gyrofrequency. Here, the first and second terms in the right-hand side of eq. (2.1) represents the adiabatic and nonadiabatic parts, respectively. The velocity vector $\boldsymbol{v}$ is written as $\boldsymbol{v} = v_\parallel \boldsymbol{b} + v_\perp(\boldsymbol{e}_1 \cos\xi + \boldsymbol{e}_2 \sin\xi)$ where ξ is the gyrophase and $(\boldsymbol{e}_1, \boldsymbol{e}_2, \boldsymbol{b})$ are the unit vectors which forms a right-hand orthogonal system at each point. The ion nonadiabatic distribution function h is independent of the gyrophase and is described in the linear, collisionless, and electrostatic case by the gyrokinetic equation[9] as

$$\left(\frac{\partial}{\partial t} + i\omega_D + ik_\parallel v_\parallel\right) h = \left(\frac{\partial}{\partial t} + i\omega_{*T}\right) \frac{e\phi}{T_i} J_0(k_\perp \rho) n_0 F_M \tag{2.2}$$

where J_0 is the Bessel function of order zero, $\omega_D \equiv \hat{\omega}_D(v_\perp^2/2 + v_\parallel^2)/v_{Ti}^2$ is the ion ∇B-curvature drift frequency, and $\omega_{*T} = \omega_{*i}[1 + \eta_i\{(v/v_{Ti})^2 - 3/2\}]$. The characteristic ion ∇B-curvature drift frequency is given by $\hat{\omega}_D \equiv 2\epsilon_n \omega_{*i}$ where $\omega_{*i} \equiv -\tau_e^{-1}\omega_{*e}$ is the ion diamagnetic drift frequency and $\epsilon_n \equiv L_n/R$ is the ratio of the equilibrium density gradient scale length $L_n \equiv -(d\ln n_0/dr)^{-1}$ to the magnetic curvature radius R. Here $\tau_e \equiv T_e/T_i$ is the ratio between the electron and ion temperatures, $\omega_{*e} \equiv ck_\theta T_e/(eBL_n)$ is the electron diamagnetic drift frequency, and k_θ is the poloidal wavenumber. The ratio of the ion temperature gradient to the density gradient is given by $\eta_i \equiv d\ln T_i/d\ln n_0$. In the gyrokinetic equation (2.2), we have used the local kinetic approximation to replace the parallel drift operator $v_\parallel \boldsymbol{b} \cdot \nabla$ with $ik_\parallel v_\parallel$ in terms of the parallel wavenumber $k_\parallel$. Here we assume that the perturbation is localized in the bad curvature region of the magnetic confinement system and, in the case of tokamaks, the ∇B-curvature drift frequency $\hat{\omega}_D \equiv 2\epsilon_n \omega_{*i}$ corresponds to the value at the outermost point of the magnetic field line on the toroidal surface. Using this local approximation for the toroidal system with a large aspect ratio, the perpendicular wavenumber is approximately given by the poloidal wavenumber as $k_\perp \simeq k_\theta$.

In order to treat the initial value problem, it is convenient to introduce the Laplace transform

$$h(\omega) = \int_0^\infty dt\, h(t) e^{i\omega t} \tag{2.3}$$

and rewrite eq. (2.2) as

$$h(\omega) = \frac{\omega - \omega_{*T}}{\omega - \omega_D - k_\parallel v_\parallel} \frac{e\phi}{T_i} J_0 n_0 F_M + i\frac{\langle \delta f_i(t=0) e^{i\boldsymbol{k}_\perp \boldsymbol{\rho}} \rangle}{\omega - \omega_D - k_\parallel v_\parallel} \tag{2.4}$$

where $\langle \cdots \rangle$ denotes the gyrophase average.

2.2 Ballistic response

Here we consider the ballistic response to the initial perturbation in the presence of the toroidal resonance, which is determined by the propagator in the left-hand side of the gyrokinetic equation (2.2). The same problem was already treated by Kim *et al.*[8] although it is reviewed here for comparison to the full initial value problem of the toroidal ITG mode shown later. Let us put $\phi = 0$ to neglect the right-hand side of the gyrokinetic equation (2.2). Then, from the inverse Laplace transform of eq. (2.4) or directly from eq. (2.2) with $\phi = 0$, we obtain

$$\begin{aligned} h(t) &= i\int_C \frac{d\omega}{2\pi} \frac{h(t=0)e^{-i\omega t}}{\omega - \omega_D - k_\parallel v_\parallel} \\ &= h(t=0)\exp[-i(\omega_D + k_\parallel v_\parallel)t]. \end{aligned} \tag{2.5}$$

The ion density perturbation is given by

$$\begin{aligned} \delta n_i(t) &= \int d^3v\, J_0(k_\perp \rho) h(t) \\ &= i\int_L \frac{d\omega}{2\pi} \int d^3v \frac{J_0(k_\perp\rho)h(t=0)e^{-i\omega t}}{\omega - \omega_D - k_\parallel v_\parallel} \\ &= \int d^3v\, J_0(k_\perp\rho) h(t=0)\exp[-i(\omega_D + k_\parallel v_\parallel)t]. \end{aligned} \tag{2.6}$$

We find in the next section how to take the contours C and L in eqs. (2.5) and (2.6).

Here, we assume the initial condition to be give by

$$h(t=0) = C_h J_0(k_\perp \rho) F_M \tag{2.7}$$

where C_h is a constant. The above form is taken in order to simplify comparison to the case of the initial value problem including self-consistent potential fluctuations considered in the next section. Then we obtain from eqs. (2.6) and (2.7),

$$\frac{\delta n(t)}{\delta n(0)} = \frac{\Gamma_0[b_i/(1 + i\hat{\omega}_D t/2)]}{\Gamma_0(b_i)} \frac{\exp[-k_\parallel^2 v_{Ti}^2 t^2/4(1 + i\hat{\omega}_D t)]}{(1 + i\hat{\omega}_D t/2)(1 + i\hat{\omega}_D t)^{1/2}} \tag{2.8}$$

where $b_i = k_\perp^2 \rho_{Ti}^2/2$, $\rho_{Ti}^2 = v_{Ti}^2/\Omega_i^2 = 2c^2 m_i T_i/(e^2 B^2)$, $\Gamma_0(b_i) = I_0(b_i)\exp(-b_i)$, and I_0 is the modified Bessel function of order zero. In the limit of $k_\perp \rho_{Ti} \to +0$, we have $\Gamma_0 \to 1$ and eq. (2.8) reduces to the result obtained by Kim *et al.*[8] The temporal dependence of the density

perturbation $\delta n(t)$ divides into two limiting cases as

$$\frac{\delta n(t)}{\delta n(0)} = \begin{cases} \exp(-{k_\parallel}^2 v_{T_i}^2 t^2/4) \\ \quad \text{for } |\hat{\omega}_D t| < 1. \\ \dfrac{2\,\exp\left[-k_\parallel^2 v_{T_i}^2/(4\hat{\omega}_D^2)\right]\exp\left[ik_\parallel^2 v_{T_i}^2 t/(4\hat{\omega}_D)\right]}{\Gamma_0(b_i)\,(i\hat{\omega}_D t)^{3/2}} \\ \quad \text{for } |\hat{\omega}_D t| > 1. \end{cases} \tag{2.9}$$

For $|\hat{\omega}_D t| < 1$, the density perturbation decays exponentially due to the phase mixing by the parallel drift provided $|k_\parallel v_{Ti}| > 2|\hat{\omega}_D|$. On the other hand, for $|\hat{\omega}_D t| > 1$, the phase mixing is dominated by the toroidal magnetic ∇B-curvature drift and the density perturbation decays according to the power law $\propto t^{-3/2}$ with oscillation at the frequency $\omega_{br} = -k_\parallel^2 v_{Ti}^2/(4\hat{\omega}_D)$ which we call the branch frequency.

§3. Time Evolution of the Toroidal ITG Mode

3.1 Formulation of the toroidal ITG mode as an initial value problem

In order to describe the toroidal ITG mode as an initial value problem, we use the Laplace-transformed ion gyrokinetic equation (2.4). Furthermore, assuming the electron density perturbation δn_e to satisfy the Boltzmann relation

$$\frac{\delta n_e}{n_0} = \frac{e\phi}{T_e} \tag{3.1}$$

and using the charge neutrality condition

$$\delta n_e = \delta n_i \tag{3.2}$$

we obtain

$$\frac{e\phi(\omega)}{T_i} = \frac{I(\omega)}{D(\omega)} \tag{3.3}$$

where

$$I(\omega) = \int d^3v \frac{iJ_0(k_\perp\rho)\langle n_0^{-1}\delta f_i(t=0)e^{i\boldsymbol{k}_\perp\cdot\boldsymbol{\rho}}\rangle}{\omega - \omega_D - k_\parallel v_\parallel} \tag{3.4}$$

$$D(\omega) = 1 + \tau_e^{-1} - \int d^3v \frac{(\omega - \omega_{*T})\,J_0^2(k_\perp\rho)F_M}{\omega - \omega_D - k_\parallel v_\parallel} \tag{3.5}$$

The dispersion relation for the toroidal ITG mode with $\boldsymbol{k} = k_\parallel \boldsymbol{b} + \boldsymbol{k}_\perp$ is given by $D(\omega) = 0$. The time evolution of the electrostatic potential is given by the inverse Laplace transform of $\phi(\omega)$ in eq. (3.3) as

$$\phi(t) = \int_L \frac{d\omega}{2\pi}\phi(\omega)e^{-i\omega t} \tag{3.6}$$

where L is a contour which lies above all of the singular points of $\phi(\omega)$ on the complex ω plane. Also, substituting eq. (3.3) into eq. (2.4) and taking its inverse Laplace transform, we can obtain the time evolution of the nonadiabatic distribution function $h(t)$.

3.2 Analytic continuation on the complex-frequency plane

In order to obtain $\phi(\omega)$ for any complex-valued frequency ω, we need to evaluate analytical continuation of the functions $I(\omega)$ and $D(\omega)$ accurately. For that purpose, we follow Kim *et al.*[8] and consider the velocity-space integral in the form of

$$P(\omega) = \int_{-\infty}^{\infty} dv_\parallel \int_0^\infty v_\perp dv_\perp \frac{g(\omega, v_\parallel, v_\perp)}{\omega + a{v_\perp}^2 + b{v_\parallel}^2 - cv_\parallel} \tag{3.7}$$

where a, b, and c are assumed to be real constants. The functions $D(\omega)$ and $I(\omega)$ both contain the same form of functions as $P(\omega)$. Also assuming a and b to be positive, we transform the velocity-space variables as

$$v_\perp' = \sqrt{a}v_\perp \qquad {v_\parallel}' = \sqrt{b}\left(v_\parallel - \frac{c}{2b}\right) \tag{3.8}$$

and

$$v' = \sqrt{({v_\perp}')^2 + ({v_\parallel}')^2}, \qquad \mu = v_\parallel'/v'. \tag{3.9}$$

Then, the function $P(\omega)$ is rewritten as

$$P(\omega) = \frac{1}{a\sqrt{b}}\int_{-1}^{1} d\mu \int_0^\infty {v'}^2 dv' \frac{G(\omega, v', \mu)}{\omega' + {v'}^2} \tag{3.10}$$

where we have defined $\omega' = \omega - c^2/4b$ and $G(\omega, v', \mu) = g[\omega, v_\parallel(v', \mu), v_\perp(v', \mu)]$ with $v_\parallel(v', \mu)$ and $v_\perp(v', \mu)$ given by the relations in eqs. (3.8) and (3.9). Apparently, the integrand has two poles $v' = \pm(-\omega')^{1/2}$ on the complex v'-plane. When ω' moves from $\omega_i' = \mathrm{Im}(\omega') > 0$ to $\omega_i' < 0$ across the ω_r'-axis with $\omega_r' = \mathrm{Re}(\omega') < 0$, one of these poles $(-\omega')^{1/2}$ with $\mathrm{Re}(-\omega')^{1/2} > 0$ crosses the v_r'-axis with $v_r' = \mathrm{Re}(v') > 0$, which corresponds to the occurrence of resonant particles. These motions of ω' and a corresponding pole $(-\omega')^{1/2}$ with $\mathrm{Re}(-\omega')^{1/2} > 0$ on the complex v'-plane are shown in Figs. 1 (a) and (b), respectively. This crossing requires the residue of the integrand at the pole to be included in $P(\omega)$ for its analytic continuation as shown in Fig. 1 (b).

On the other hand, when ω' moves from $\omega_i' > 0$ to $\omega_i' < 0$ across the ω_r'-axis with $\omega_r' > 0$, the two poles neither cross the v_r'-axis nor make any residue's contributions to $P(\omega)$. Then, we make a branch cut from $\omega' = 0$ along the ω_i'-axis with $\omega_i' < 0$ as shown in Fig. 1 (a) and write $P(\omega)$ as

$$P(\omega) = \begin{cases} P_0(\omega) & \text{in I, II, and IV} \\ P_0(\omega) + \Delta_P(\omega) & \text{in III} \end{cases} \tag{3.11}$$

where I–IV represent the regions on the complex ω'-plane shown by Fig. 1 (a) and $P_0(\omega)$ denotes the contribution from the straight integration contour, which is given by eq. (3 10) with the v'-integration along the v_r'-axis with $v_r' > 0$. The residue's contribution $\Delta_P(\omega)$ is written as

$$\Delta_P(\omega) = -\pi i \frac{(-\omega')^{1/2}}{a\sqrt{b}}\int_{-1}^{1} d\mu\, G[\omega, v' = (-\omega')^{1/2}, \mu]. \tag{3.12}$$

The condition $\omega' = 0$ gives $\omega = c^2/4b \equiv \omega_{br}$ which is called the branch frequency. In the limit of $\omega \to \omega_{br}$, we

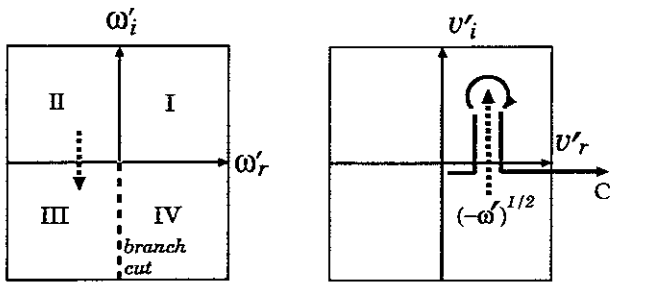

Fig. 1(a) Fig. 1(b)

Fig. 1. Motions of the complex frequency $\omega' = \omega - c^2/4b$ on the complex ω'-plane (a) and the corresponding pole $(-\omega')^{1/2}$ with $\mathrm{Re}(-\omega')^{1/2} > 0$ in the complex v'-plane (b). When ω' moves from $\omega_i' = \mathrm{Im}(\omega') > 0$ to $\omega_i' < 0$ across the ω_r'-axis with $\omega_r' = \mathrm{Re}(\omega') < 0$, the pole $(-\omega')^{1/2}$ with $\mathrm{Re}(-\omega')^{1/2} > 0$ crosses the v_r'-axis with $v_r' = \mathrm{Re}(v') > 0$. A branch cut is taken from $\omega' = 0$ along the ω_i'-axis with $\omega_i' < 0$ as shown by a dashed line in (a).

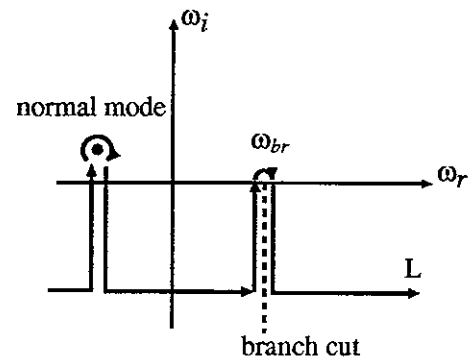

Fig. 2. The integration contour L on the complex ω-plane for evaluating the inverse Laplace transform (3.3). Dominant contributions to the integral are made by poles and a branch cut.

obtain from eqs. (3.10)–(3.12)

$$P_0(\omega) \to P(\omega_{br}) = \frac{1}{a\sqrt{b}} \int_{-1}^{1} d\mu \int_0^{\infty} dv' G(\omega, v', \mu) \tag{3.13}$$

$$\Delta_P(\omega) \simeq -\pi i \frac{(\omega_{br} - \omega)^{1/2}}{a\sqrt{b}} \int_{-1}^{1} d\mu\, G[\omega, v' = 0, \mu]. \tag{3.14}$$

3.3 Normal modes and a continuum mode

For analytic continuation of $\phi(\omega)$ given by eq. (3.3), we need to take account of the poles defined by $D(\omega) = 0$ and the branch cut growing from the branch frequency ω_{br}. Comparing eqs. (3.4) and (3.5) with eq. (3.7), we obtain $2a = b = -\hat{\omega}_D/v_{Ti}^2$ and $c = k_\parallel$ where $\hat{\omega}_D \equiv 2\epsilon_n \omega_{*i} < 0$ is assumed. Then, the branch frequency is written as $\omega_{br} = c^2/4b = -k_\parallel^2 v_{Ti}^2/(4\hat{\omega}_D)$. For evaluating the inverse Laplace transform (3.3), we take the integration contour L as shown in Fig. 2.

For $t > 0$, $\phi(t)$ is written as the sum of the contributions from the poles (normal modes) and the branch cut:

$$\phi(t) = \phi_p(t) + \phi_{br}(t) \tag{3.15}$$

where the poles' (or normal modes') contribution is given by

$$\frac{e\phi_p(t)}{T_i} = -i \sum_n \frac{I(\omega_n)}{\frac{dD}{d\omega}(\omega_n)} e^{-i\omega_n t} \tag{3.16}$$

and the contribution from the branch cut is written as

$$\begin{aligned} \frac{e\phi_{br}(t)}{T_i} &= \int_{C_{br}} \frac{d\omega}{2\pi} e^{-i\omega t} \left(\frac{I_0 + \Delta_I}{D_0 + \Delta_D} - \frac{I_0}{D_0} \right) \\ &= ie^{-i\omega_{br} t} \int_{-\infty}^{0} \frac{d\omega_i}{2\pi} e^{\omega_i t} \left. \frac{D_0 \Delta_I - I_0 \Delta_D}{D_0 (D_0 + \Delta_D)} \right|_{\omega_r = \omega_{br}} \end{aligned} \tag{3.17}$$

The normal-mode frequencies ω_n in eq. (3.16) are determined by $D(\omega_n) = 0$. In eq. (3.17), the branch cut C_{br} is taken as the straight line path from $\omega_{br} - i\infty$ to $\omega_{br} - i0$ and the functions $D_0(\omega)$, $I_0(\omega)$, $\Delta_D(\omega)$, and $\Delta_I(\omega)$ are defined in the same way as $P_0(\omega)$ and $\Delta_P(\omega)$ in eqs. (3.11) and (3.12). Thus $\Delta_D(\omega)$ and $\Delta_I(\omega)$ represent contributions from the resonant pole in the velocity space shown by Fig. 1 (b) and are written as

$$\Delta_I = 4\pi^2 \frac{(\omega_{br} - \omega)^{\frac{1}{2}}}{(-\hat{\omega}_D)^{\frac{3}{2}}} \int_{-1}^{1} d\mu\, \frac{J_0}{n_0} \left\langle \delta f_i (t = 0) e^{i \boldsymbol{k}_\perp \cdot \boldsymbol{\rho}} \right\rangle \Big|_{v' = v_0'} \tag{3.18}$$

and

$$\Delta_D = 4\pi^2 i \frac{(\omega_{br} - \omega)^{\frac{1}{2}}}{(-\hat{\omega}_D)^{\frac{3}{2}}} \int_{-1}^{1} d\mu\, (\omega - \omega_{*T})\, J_0^2 F_M \Big|_{v' = v_0'} \tag{3.19}$$

respectively, where we have transformed the velocity variables as in eqs. (3.8) and (3.9), and where $v_0' = (\omega_{br} - \omega)^{1/2}$.

As shown in eqs. (3.13) and (3.14) in the limit of $\omega \to \omega_{br}$, we have $D_0(\omega) \to D(\omega_{br})$, $I_0(\omega) \to D(\omega_{br})$, $\Delta_D(\omega) \simeq C_D(\omega_{br} - \omega)^{1/2}$, and $\Delta_I(\omega) \simeq C_I(\omega_{br} - \omega)^{1/2}$ where C_D and C_I are constants. Then, from eq. (3.17), we obtain the asymptotic behavior of the branch cut contribution to the potential as

$$\frac{e\phi_{br}(t)}{T_i} \simeq t^{-3/2} e^{-i\omega_{br} t} \frac{e^{i3\pi/4}}{4\sqrt{\pi}} \left[\frac{C_I}{D(\omega_{br})} - \frac{C_D I(\omega_{br})}{\{D(\omega_{br})\}^2} \right] \tag{3.20}$$

for $t \gg -1/\hat{\omega}_D$, where

$$\begin{aligned} C_I &= \frac{8\pi^2}{(-\hat{\omega}_D)^{3/2}} \frac{v_{Ti}^3}{n_0} \delta f_i \left(t = 0, v_\perp = 0, v_\parallel = -\frac{k_\parallel v_{Ti}^2}{2\hat{\omega}_D} \right) \\ C_D &= \frac{8\pi^{1/2} i}{(-\hat{\omega}_D)^{3/2}} \left[\omega_{br} - \omega_{*i} \left\{ 1 + \eta_i \left(\frac{k_\parallel^2 v_{Ti}^2}{4\hat{\omega}_D^2} - \frac{3}{2} \right) \right\} \right] \\ &\quad \cdot \exp\left(-\frac{k_\parallel^2 v_{Ti}^2}{4\hat{\omega}_D^2} \right). \end{aligned} \tag{3.21}$$

Noting that $\delta n_i = \delta n_e = n_0 e\phi/T_e$ and comparing eq. (3.20) with eq. (2.9), we see that, for the initial value problem of the toroidal ITG mode, the potential and

density perturbations derived from the branch cut integration show the same form of asymptotic behavior $\propto t^{-3/2}e^{-i\tilde{\omega}_{br}t}$ as the the density perturbation for the ballistic mode without interaction with the potential. [If we put $D_0(\omega) = 1$ with $\Delta_D = 0$ in eq. (3 17), the ballistic mode case in eq (2.6) is reproduced.]

Now we find from eqs. (3.15), (3.16), and (3 20) that the long-time asymptotic behavior of the potential and density perturbations for the toroidal ITG mode is determined by the normal mode with the largest positive growth rate for the unstable case while it is dominated by the continuum mode for the stable case in which all normal modes decay faster than the continuum mode.

It should be remarked here that there is some arbitrariness about how to make a branch cut from the branch frequency. Different branch cuts make differences in definitions of $\phi_p(t)$ and $\phi_{br}(t)$ because of changes in complex-frequency regions where analytic continuation of $D(\omega)$ and $I(\omega)$ is defined. However, it is obvious that the total perturbation $\phi(t) = \phi_p(t) + \phi_{br}(t)$ and its asymptotic behavior given by eq. (3.20) for the stable case should be independent of the way to make a branch.

§4. Numerical examples

4.1 Dispersion relation

Following the prescription given in the previous section, we can calculate the dispersion function $D(\omega)$ analytically continued on the whole complex ω-plane. Here the dispersion relation $D(\omega) = 0$ is numerically solved to obtain the eigenfrequency $\omega_n = \omega_r + i\gamma$ of the normal mode. Figure 3 shows the resultant normalized growth rate $L_n\gamma/v_{Ti}$ and real frequency $L_n\omega_r/v_{Ti}$ of the toroidal ITG mode as a function of the normalized poloidal wavenumber $k_\theta\rho_{Ti}$ for $\tau_e = 1$, $\epsilon_n = 0.25$, $\eta_i = 2.5$, and $k_\parallel R = 1/3, 1/2, 1$. We can see that, owing to the proper analytic continuation, the growth rate and real frequency are smoothly continued into the stable regions where the growth rate is negative. The stable regions are found for both small and large poloidal wavenumbers. Also, the growth rate decreases with the parallel wavenumber increased. For all curves shown in Fig. 3, the real frequency is smaller than the branch frequency so that the toroidal resonance is essential to the dispersion relation. The growth rate and real frequency for the nonresonant mode are not shown in Fig. 3.

Figure 4 shows the normalized growth rate $L_n\gamma/v_{Ti}$ (top) and real frequency $L_n\omega_r/v_{Ti}$ (bottom) of the toroidal ITG mode as a function of η_i for $\tau_e = 1$, $k_\theta\rho_{Ti} = 0.75$, $k_\parallel R = 1/2$, and $\epsilon_n = 0.1, 0.25, 0.4$. We can see that the growth rate increases with increasing η_i and that the real frequency has the negative sign corresponding to the ion diamagnetic rotation for larger values of η_i. Since we are able to calculate negative growth rates, we can clearly identify the critical η_i value which is shown in Fig 4 to increase with increasing ϵ_n.

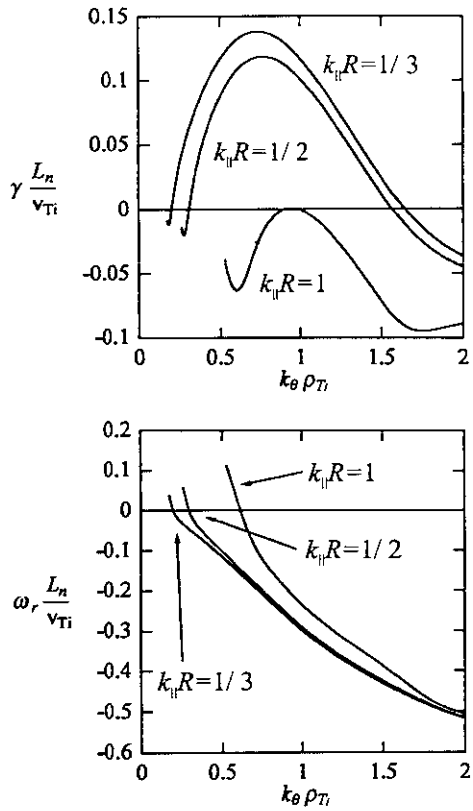

Fig. 3. The normalized growth rate $L_n\gamma/v_{Ti}$ (top) and real frequency $L_n\omega_r/v_{Ti}$ (bottom) of the toroidal ITG mode as a function of the normalized poloidal wavenumber $k_\theta\rho_{Ti}$ for $\tau_e = 1$, $\epsilon_n = 0.25$, $\eta_i = 2.5$, and $k_\parallel R = 1/3, 1/2, 1$.

4.2 Solution of the initial value problem

Here let us consider an example of the initial value problem in which the initial perturbation is proportional to Maxwellian. Then, we use the same initial condition for the nonadiabatic distribution as in eq. (2.7) to obtain a compact expression for the gyrophase-averaged initial distribution function in eq. (3.4) as

$$\langle \delta f_i(t=0) e^{-i\boldsymbol{k}_\perp \cdot \boldsymbol{\rho}} \rangle = C_f J_0(k_\perp \rho) F_M \, \delta n(t=0) \quad (4.1)$$

with

$$C_f = -\tau_e + (1+\tau_e)/\Gamma_0(b_i) \quad (4.2)$$

where (2.1),(3.1) and (3.2) are used. We have $C_f \to 1$ in the small gyroradius limit $k_\perp\rho_{Ti} \to +0$. The density and potential perturbation at $t > 0$ are given by using eqs. (3.4),(3.5),(3.15)-(3.19), and the initial condition (4.1).

Figure 5 shows time evolution of the toroidal ITG mode for the stable case where $\tau_e = 1$, $\epsilon_n = 0.25$, $\eta_i = 2.5$, $k_\parallel R = 0.5$, and $k_\theta\rho_{Ti} = 0.28$. In this case, the eigenfrequency of the normal mode and the branch frequency are given by $L_n\omega_n/v_{Ti} = 0.024 - 0.019i$ and $L_n\omega_{br}/v_{Ti} = 0.056$. The potential amplitudes of the normal mode $\phi_p(t)$ (a solid curve) and the continuum mode $\phi_{br}(t)$ (a dotted curve) are shown in Fig. 5 (a). The total potential $\phi(t) = \phi_p(t) + \phi_{br}(t)$ is shown in Fig. 5 (b). The asymptotic behavior is well described by the Analytical result given by eq. (3.20) which is shown by the dashed

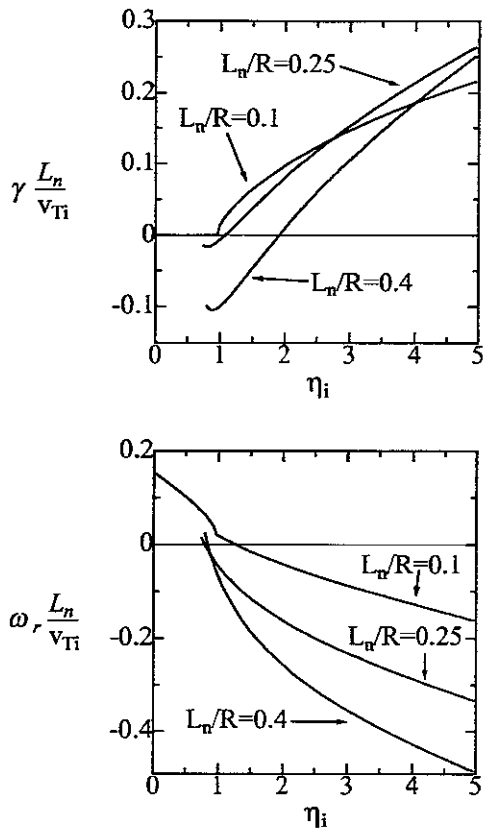

Fig. 4. The normalized growth rate $L_n\gamma/v_{Ti}$ (top) and real frequency $L_n\omega_r/v_{Ti}$ (bottom) of the toroidal ITG mode as a function of η_i for $\tau_e = 1$, $k_\theta\rho_{Ti} = 0.75$, $k_\parallel R = 1/2$, and $\epsilon_n = 0.1, 0.25, 0.4$.

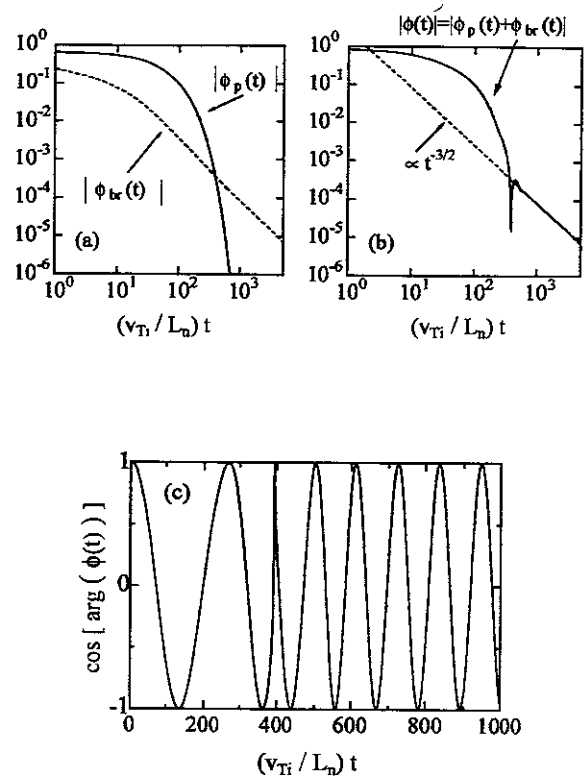

Fig. 5. Time evolution of the toroidal ITG mode for the stable case where $\tau_e = 1$, $\epsilon_n = 0.25$, $\eta_i = 2.5$, $k_\parallel R = 0.5$, and $k_\theta\rho_{Ti} = 0.28$. (a) The potential amplitudes of the normal mode $\phi_p(t)$ (a solid curve) and the continuum mode $\phi_{br}(t)$ (a dotted curve). (b) The total potential $\phi(t) = \phi_p(t) + \phi_{br}(t)$ normalized by the initial value $\phi(t=0)$. (c) The cosine of the phase of the potential $\phi(t)$. Here the eigenfrequency of the normal mode and the branch frequency are given by $L_n\omega_n/v_{Ti} = 0.024 - 0.019i$ and $L_n\omega_{br}/v_{Ti} = 0.056$. The dashed line in (b) represents the analytical result given by eq. (3.20) for the asymptotic limit.

line in Fig. 5 (b). The cosine of the phase of the potential $\phi(t)$ is given in Fig. 5 (c) which clearly shows the change from the normal mode frequency to the branch frequency. Note that Figs. 5 (a)–(c) also show the behavior of the density perturbation because $\delta n_e = \delta n_i = n_0 e\phi/T_e$.

We find from these figures that, for the stable case, the temporal behavior of the ITG mode is described by the exponential dependence of the normal mode only near the initial time although the long-time asymptotic behavior is dominantly determined by the power-law decay of the continuum mode.

Generally, the number of the normal modes for given parameters is more than one. Figures 3 and 4 show the growth rate and real frequency for the most unstable (or the least stable) normal mode. For the parameters used in Fig. 5, there exist an infinite number of stable normal modes with eigenfrequencies $L_n\omega_n/v_{Ti} = 0.024 - 0.019i$, $-0.073 - 0.103i$, $-0.463 - 0.565i$, $\cdots$. However only the least stable normal mode is used in Fig. 5 since the results in Fig. 5 change little even if other rapidly decaying normal modes are added.

§5. Conclusions

In this work, temporal evolution of the toroidal ITG mode has been studied by solving the initial value problem of the ion gyrokinetic equation combined with the electron Boltzmann relation and the charge neutrality condition.

For the toroidal ITG mode, temporal dependence of the density and potential perturbations is described by two types of behavior. One is well-known normal modes which change exponentially in time. Their frequencies and growth rates are determined by the dispersion relation and correspond to the poles of the Laplace-transformed potential function on the complex frequency plane. The other type is a continuum mode which is given by the integration of the Laplace-transformed potential function along a branch cut. Occurrence of the branch cut is due to the quadratic velocity dependence of the toroidal ∇B-curvature drift. The long-time asymptotic behavior of the continuum mode is characterized by oscillation at the branch frequency and power law decay

$\propto t^{-3/2}$. This behavior is the same as that of the ballistic response obtained by the propagator of the gyrokinetic equation without taking account of interaction with the potential.

If the normal mode analysis shows the system to be unstable, the long-time behavior is dominantly described by the normal mode with the largest growth rate. On the other hand, when the system is stable, only the normal modes are not enough for describing the temporal evolution of the toroidal ITG mode. In the stable case, the system is eventually dominated by the continuum mode since all the normal modes decay more rapidly.

In the future, we consider the fields associated with the test gyrokinetic particle. The noise associated with an ensemble of statistical independent dressed test gyrokinetic particles may be of importance for computer simulations of ITG turbulence.

Acknowledgements

The authors thank Dr. Y. Kishimoto for helpful discussions.

1) L. I. Rudakov and R. Z. Sagdeev: Sov. Phys.-Dokl. 6 (1961) 415.
2) W. Horton and R. K. Varma. Phys. Fluids 15 (1972) 620.
3) C. Z. Cheng and K. T. Tsang: Nucl. Fusion 21 (1981) 643.
4) F. Romanelli: Phys. Fluids B 1 (1989) 1018.
5) J. Y. Kim and W. Horton: Phys. Fluids B 3 (1991) 1167.
6) J. Q. Dong, W. Horton, and J. Y. Kim: Phys. Fluids B 4 (1992) 1867.
7) T. Yamagishi: *Cross-Field Energy Flux due to Ion Temperature Gradient Mode in a Tokamak*, US-Japan Workshop on Ion Temperature Gradient-Driven Turbulent Transport, ed. W. Horton, M. Wakatani, and A. Wootton, AIP Conference Proceedings No. 284 (1993) p. 428.
8) J. Y. Kim, Y. Kishimoto, W. Horton, and T. Tajima: Phys. Plasmas 1 (1994) 927.
9) R. D. Hazeltine and J. D. Meiss: *Plasma Confinement* (Addison-Wesley, Redwood City, CA, 1992) p.123.
10) P. Similon, J. E. Sedlak, D. Stotler, H. L. Berk, W. Horton, and D. Choi: J. Comput. Phys.54 (1984) 260.

Recent Issues of NIFS Series

NIFS-515 K Akaishi,
On the Solution of the Outgassing Equation for the Pump-down of an Unbaked Vacuum System, Oct 1997

NIFS-516 *Papers Presented at the 6th H-mode Workshop (Seeon, Germany)*; Oct 1997

NIFS-517 John L. Johnson,
The Quest for Fusion Energy; Oct. 1997

NIFS-518 J. Chen, N. Nakajima and M. Okamoto,
Shift-and-Inverse Lanczos Algorithm for Ideal MHD Stability Analysis; Nov. 1997

NIFS-519 M. Yokoyama, N Nakajima and M. Okamoto,
Nonlinear Incompressible Poloidal Viscosity in L=2 Heliotron and Quasi-Symmetric Stellarators; Nov. 1997

NIFS-520 S. Kida and H Miura,
Identificaiton and Analysis of Vortical Structures; Nov. 1997

NIFS-521 K. Ida, S. Nishimura, T Minami, K. Tanaka, S. Okamura, M Osakabe, H Idei, S. Kubo, C Takahashi and K. Matsuoka,
High Ion Temperature Mode in CHS Heliotron/torsatron Plasmas, Nov. 1997

NIFS-522 M Yokoyama, N. Nakajima and M. Okamoto,
Realization and Classification of Symmetric Stellarator Configurations through Plasma Boundary Modulations; Dec 1997

NIFS-523 H. Kitauchi,
Topological Structure of Magnetic Flux Lines Generated by Thermal Convection in a Rotating Spherical Shell; Dec. 1997

NIFS-524 T. Ohkawa,
Tunneling Electron Trap; Dec. 1997

NIFS-525 K. Itoh, S.-I. Itoh, M. Yagi, A. Fukuyama,
Solitary Radial Electric Field Structure in Tokamak Plasmas, Dec. 1997

NIFS-526 Andrey N. Lyakhov,
Alfven Instabilities in FRC Plasma; Dec. 1997

NIFS-527 J. Uramoto,
Net Current Increment of negative Muonlike Particle Produced by the Electron and Positive Ion Bunch-method; Dec. 1997

NIFS-528 Andrey N. Lyakhov,
Comments on Electrostastic Drift Instabilities in Field Reversed Configuraiton; Dec. 1997

NIFS-529 J. Uramoto,
Pair Creation of Negative and Positive Pionlike (Muonlike) Particle by Interaction between an Electron Bunch and a Positive Ion Bunch; Dec. 1997

NIFS-530 J. Uramoto,
Measuring Method of Decay Time of Negative Muonlike Particle by Beam Collector Applied RF Bias Voltage; Dec. 1997

NIFS-531 J Uramoto,
Confirmation Method for Metal Plate Penetration of Low Energy Negative Pionlike or Muonlike Particle Beam under Positive Ions; Dec. 1997

NIFS-532 J Uramoto,
Pair Creations of Negative and Positive Pionlike (Muonlike) Particle or K Mesonlike (Muonlike) Particle in H2 or D2 Gas Discharge in Magnetic Field; Dec. 1997

NIFS-533 S. Kawata, C. Boonmee, T. Teramoto, L. Drska, J. Limpouch, R. Liska, M Sinor,
Computer-Assisted Particle-in-Cell Code Development; Dec 1997

NIFS-534 Y. Matsukawa, T. Suda, S. Ohnuki and C. Namba,
Microstructure and Mechanical Property of Neutron Irradiated TiNi Shape Memory Alloy; Jan. 1998

NIFS-535 A. Fujisawa, H. Iguchi, H. Idei, S. Kubo, K. Matsuoka, S. Okamura, K. Tanaka, T. Minami, S. Ohdachi, S. Morita, H. Zushi, S. Lee, M. Osakabe, R. Akiyama, Y. Yoshimura, K. Toi, H. Sanuki, K. Itoh, A. Shimizu, S. Takagi, A. Ejiri, C. Takahashi, M. Kojima, S. Hidekuma, K. Ida, S. Nishimura, N. Inoue, R. Sakamoto, S.-I. Itoh, Y. Hamada, M. Fujiwara,
Discovery of Electric Pulsation in a Toroidal Helical Plasma; Jan. 1998

NIFS-536 Lj.R. Hadzievski, M.M. Skoric, M. Kono and T. Sato,
Simulation of Weak and Strong Langmuir Collapse Regimes; Jan. 1998

NIFS-537 H. Sugama, W. Horton,
Nonlinear Electromagnetic Gyrokinetic Equation for Plasmas with Large Mean Flows; Feb. 1998

NIFS-538 H. Iguchi, T.P. Crowley, A. Fujisawa, S. Lee, K. Tanaka, T Minami, S. Nishimura, K. Ida, R. Akiyama, Y Hamada, H., Idei. M. Isobe, M. Kojima, S. Kubo, S. Morita, S. Ohdachi, S. Okamura, M. Osakabe, K. Matsuoka, C Takahashi and K. Toi,
Space Potential Fluctuations during MHD Activities in the Compact Helical System (CHS); Feb. 1998

NIFS-539 Takashi Yabe and Yan Zhang,
Effect of Ambient Gas on Three-Dimensional Breakup in Coronet Formation Process; Feb. 1998

NIFS-540 H. Nakamura, K. Ikeda and S. Yamaguchi,
Transport Coefficients of InSb in a Strong Magnetic Field; Feb. 1998

NIFS-541 J. Uramoto,
Development of ν_μ Beam Detector and Large Area ν_μ Beam Source by H_2 Gas Discharge (I); Mar 1998

NIFS-542 J. Uramoto,
Development of $bar\{\nu\}_\mu$ Beam Detector and Large Area $bar\{\nu\}_\mu$ Beam Source by H_2 Gas Discharge (II); Mar. 1998

NIFS-543 J. Uramoto,
Some Problems inside a Mass Analyzer for Pions Extracted from a H_2 Gas Discharge; Mar. 1998

NIFS-544 J. Uramoto,
Simplified ν_μ $bar\{\nu\}_\mu$ Beam Detector and ν_μ $bar\{\nu\}_\mu$ Beam Source by Interaction between an Electron Bunch and a Positive Ion Bunch; Mar. 1998

NIFS-545 J. Uramoto,
Various Neutrino Beams Generated by D_2 Gas Discharge; Mar.1998

NIFS-546 R. Kanno, N. Nakajima, T. Hayashi and M. Okamoto,
Computational Study of Three Dimensional Equilibria with the Bootstrap Current; Mar. 1998

NIFS-547 R. Kanno, N. Nakajima and M. Okamoto,
Electron Heat Transport in a Self-Similar Structure of Magnetic Islands; Apr. 1998

NIFS-548 J.E. Rice,
Simulated Impurity Transport in LHD from MIST; May 1998

NIFS-549 M.M. Skoric, T. Sato, A.M. Maluckov and M.S. Jovanovic,
On Kinetic Complexity in a Three-Wave Interaction; June 1998

NIFS-550 S. Goto and S. Kida,
Passive Saclar Spectrum in Isotropic Turbulence: Prediction by the Lagrangian Direct-interaction Approximation; June 1998

NIFS-551 T. Kuroda, H. Sugama, R. Kanno, M. Okamoto and W. Horton,
Initial Value Problem of the Toroidal Ion Temperature Gradient Mode ; June 1998